Overlayer resonance and quantum well state of Cs/Cu(111) studied with angle-resolved photoemission, LEED, and first-principles calculations

M. Breitholtz,[1] V. Chis,[2] B. Hellsing,[2] S.-Å. Lindgren,[1] and L. Walldén[1]
[1]*Applied Physics Department, Chalmers University of Technology, SE-412 96 Göteborg, Sweden*
[2]*Physics Department, Göteborg University, SE-412 96 Göteborg, Sweden*
(Received 6 December 2006; published 4 April 2007)

Angle-resolved photoemission spectroscopy and low-energy electron diffraction are used to study submonolayer coverages of Cs on Cu(111) at room temperature (RT) and 170 K. At RT, the Cs saturation coverage is approximately 90% of the full monolayer coverage. The full monolayer is characterized by a quantum well state (QWS) band having an energy of 25 meV below the Fermi level (E_F) in the $\bar{\Gamma}$ point and a resonance band extending to energies below the Cu band gap. This is supported by our first-principles calculations. Low-energy electron diffraction shows that the Cs overalyer forms a (2×2) structure over a wide coverage range, in which the QWS has energies from 50 meV above to 25 meV below E_F. The continued energy shift of the QWS after saturation of the diffraction angles is interpreted in terms of vacancies in the overlayer.

DOI: 10.1103/PhysRevB.75.155403 PACS number(s): 79.60.−i, 73.21.Fg, 73.20.At, 71.15.Mb

I. INTRODUCTION

Alkali-metal overlayers attract interest as prototype examples of simple metal quantum wells, in which valence electrons are more or less confined depending on the choice of substrate.[1] Strong confinement is obtained when the substrate has a band gap, which allows a state in the overlayer to have only an oscillating tail on the substrate side of the interface. If, as exemplified by Na/Al(111), there is a potential step at the interface to a more attractive potential in the substrate, the confinement is weaker but still sufficient for resonances to be observed by photoemission or inverse photoemission.[2,3] Alkali metals on Cu(111) give examples of both strong and weak confinements. It is strong for energies within the Cu band gap at the L point of the Brillouin zone. Since this gap extends 0.75 eV below the Fermi energy[4] and the filled bandwidth of an alkali metal is appreciably larger than this, most of the valence electrons in an adsorbed film are found in resonances. The states within the gap give narrow lines in angle-resolved photoemission spectroscopy (ARPES), as noted for Na (Ref. 5) and Li,[6] and narrow onsets in dI/dV curves recorded with scanning tunneling spectroscopy (STS), as observed for Na.[7] A detailed characterization of the electron structure has also been done for the system Na/Cu(111) applying first-principles methods.[8] The calculated properties are consistent with experiment.

In a report including dI/dV data, it was recently noted for (2×2) ordered Na and Cs monolayers on Cu(111) that there is actually no strict confinement of states within the gap.[9] This follows from the different periodicities of the overlayer and the substrate. In this case, a state, which extends across the border of the two, adjusts to both periods. This is the situation for many systems, in particular, low-dimensional ones.[10] In the case of a (2×2) monolayer on Cu(111), the adjustment to two periods makes the quantum well leaky due to overlap with Cu bulk states when these are back folded into the smaller Brillouin zone defined by the overlayer. A quantum well state (QWS) at the center of the surface Brillouin zone with an energy in the lower half of the gap will overlap with Cu s,p-band bulk states along the L-X direction. This gives a small resonant width, which was estimated theoretically to be somewhat less than 10 meV. If this is correct, it explains why the dI/dV onset, which was recorded at 5 K, is broader than the calculated lifetime width of a strictly confined and, thus, discrete state in a (2×2) monolayer.

Characteristic of alkali-metal monolayers on Cu(111) is that energies of surface located states gradually shift with coverage. This applies to the surface state of Cu(111) 0.4 eV below E_F,[11,12] as well as to the strongly confined quantum well state that becomes populated at high monolayer coverage.[14,13] The ability to tune the electronic structure and properties has been manifested and exploited in a number of different experiments, where various aspects of the interaction between radiation and matter are studied.[15–17]

In the present work, we use ARPES at low photon energy to monitor the states characteristic of Cs monolayers at different coverages and of a full Cs monolayer exposed to oxygen.[25] The effect of exposing the Cs overlayer to oxygen has previously been studied. These studies were, however, limited to very small Cs coverages using ARPES and electron-energy-loss spectroscopy combined with work-function measurements for Cs coverages in the monolayer coverage range. It was suggested that oxygen acts as a diluter of the electron gas in the Cs layer, a picture which is supported by the present work.

Regarding the Cu(111) surface state, we note that it shifts upon Cs deposition to energies below the edge of the L gap, suggesting that the surface state at high coverage ends up as a monolayer resonance. This interpretation is supported by our first-principles calculations. Qualitatively, the same electronic structure is obtained, however, not discussed, in a recent calculation for Na/Cu(111).[7]

A recent scanning tunneling microscopy (STM) investigation,[24] with the sample at room temperature (RT) during the Cs deposition but at 9 K during imaging, revealed a commensurate low coverage phase with a very large distance (11 Å) between Cs atoms and well described as a $(\sqrt{19}\times\sqrt{19})$ $R23.4°$ structure. At intermediate coverages, the observed incommensurate hexagonal structures are some-

what rotated with respect to the substrate surface lattice. The reciprocal lattice vectors of these structures will mediate a coupling to Cu bulk states, as do the scattering vectors of the particular overlayer discussed by Corriol *et al.*,[9] and this will give the downshifted Cu surface state a resonant width as Cs is adsorbed.

The present experiments were made with the sample at 295 K (RT) and around 170 K. We find that the linewidth of the QWS does not depend significantly on the coverage and, thus, not on whether or not the overlayer has an ideal (2 $\times$2) structure. The state is robust even with respect to oxygen exposure and shifts to higher energies gradually with increasing oxygen exposure.

The paper is organized as follows. First, in Sec. II, we describe the experimental and theoretical methods used. In Sec. III, we outline briefly our results. The results will be discussed in more detail in Sec. IV and, finally, we make some concluding remarks in Sec. V.

II. EXPERIMENTAL AND CALCULATIONAL METHODS

Cs was evaporated onto the Cu(111) crystal from a heated Cs glass ampoule broken *in situ* and kept at constant temperature during an experimental run such that a full monolayer is obtained after 100–350 s evaporation time. All of the photoemission spectra presented below were recorded with a spectrometer (Leybold) designed for high-resolution electron-energy-loss spectroscopy and a 1 mW He-Cd laser ($h\nu$=3.82 eV) as light source. The light was made incident at an angle of 80°. Only *p*-polarized light gave off an emission from the states studied so this is the polarization used to record the presented spectra. The sample was cooled via its holder, which was attached to a LN_2 container. The sample temperature was obtained by fitting the high-energy cutoff to the Fermi-Dirac distribution in spectra where no QWS is close to the Fermi level. For a range of coverages, the QWS of interest lies above the Fermi level. The QWS is then observed as a shoulder in the raw spectra, but a peak may be recovered by multiplying the raw spectra by the inverse of the Fermi-Dirac (FD) distribution function as exemplified by the spectra in Fig. 1. When this procedure has been used, the spectra presented are labeled FD normalized.

The electronic structure calculations were performed with the total energy, plane-wave code PWSCF,[18] which is based on the density-functional theory. We adopt ultrasoft[19] pseudopotentials for Cu and Cs and the general gradient approximation[20] GGA-PBE for the exchange and correlation energy functional. A kinetic-energy cutoff of 30 Ry was used for the plane waves and a charge density cutoff energy of 480 Ry. In general, the charge-density cutoff is about four times the kinetic-energy cutoff. However, ultrasoft pseudopotentials require a substantially higher value.[21] The Brillouin-zone sampling was done over several uniform Monkhorst-Pack grids, and a finite temperature smearing of first-order Methfessel-Paxton[22] type was used with a Fermi distribution broadening ranging from σ=0.136 to σ =0.680 eV. The atomic arrangement of the (2 $\times$2)-Cs/Cu(111) was obtained by minimizing the total energy with respect to the positions of the Cs atoms in the overlayer and the Cu atoms in a slab. The supercell was built by including ten Cu layers with four Cu atoms in each layer. The Cs atoms were placed on both sides of the copper slab. In order to exclude any surface to surface interaction through the vacuum region, the surfaces are separated by 25.3 Å of vacuum. During the relaxation process, the Cu atoms where free to move in all directions, whereas the Cs atoms where restricted to move along the surface normal. The electronic band structure was calculated along the high-symmetry directions $\bar{K}$-$\bar{\Gamma}$-$\bar{M}$. Sampling was performed over 130 **k** points in a non-self-consistent manner using the self-consistent electron density obtained by optimizing the atomic arrangement.

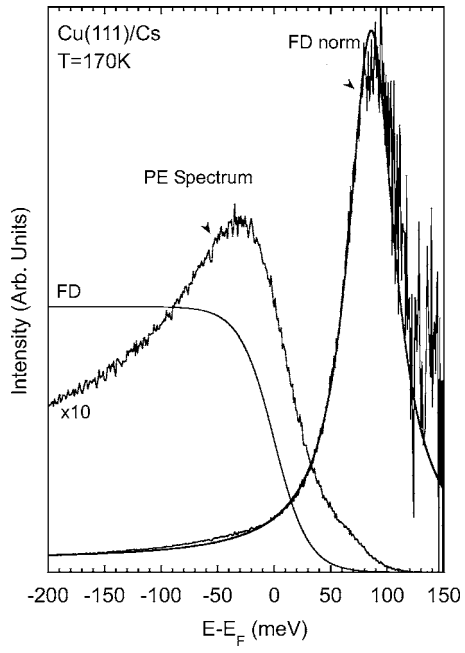

FIG. 1. The spectrum labeled PE Spectrum is recorded for a Cs coverage such that a QWS lies 85 meV above the Fermi level. The QWS is seen as a weak shoulder around 70 meV above E_F. By dividing the spectrum with the Fermi-Dirac function, given by the line labeled FD, the line FD norm is obtained. This line has a distinct peak above E_F, which can be fitted with a Lorentzian line, also shown in the diagram.

III. RESULTS

A. Coverage and temperature dependence of QWS

A QWS monitored along the surface normal shifts to lower energy as the Cs coverage is increased and saturates at around 25 meV below the Fermi energy (Fig. 2). The QWS energy changes almost linearly with the evaporation time (Fig. 3). Initially, upon continued deposition, the energy remains nearly constant while the emission line broadens. Assuming that the energy of the QWS saturates at full monolayer coverage, one thus gets a clear demarcation of this coverage. We present this observation first since the low-energy electron diffraction (LEED) pattern and the surface-state data are less distinct in this respect. At coverages for which the state is above E_F, the emission line is modified by

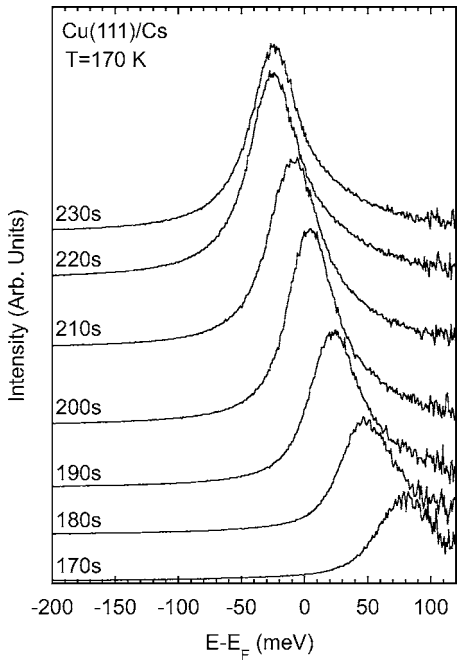

FIG. 2. Fermi-Dirac normalized photoemission spectra recorded along the surface normal for various Cs evaporation times. The evaporation time is given by each spectrum, and a complete Cs monolayer is obtained after 220 s of evaporation.

the FD cutoff function, but a peak is recovered when the raw spectra are multiplied by the inverse of the FD distribution (Fig. 1).

Figure 2 shows a plot of FD normalized spectra recorded at different Cs coverages as given by the evaporation time. The substrate temperature is 170 K. If the substrate is kept at RT, the QWS saturation energy is around 10 meV above the Fermi energy. If the sample is cooled to 170 K after saturation has been reached, the emission line narrows from a full width at half maximum (FWHM) of 57 to 40 meV, but the energy remains nearly the same (Fig. 4). Upon a small additional Cs deposited onto the cooled sample, a further downshift by around 20 meV is observed, indicating that the saturation coverage is higher at 170 K than at RT.

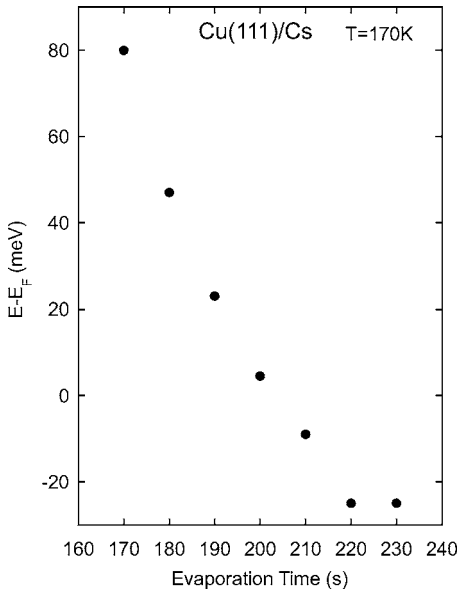

FIG. 3. Energy of the QWS plotted against the Cs evaporation time. For a full Cs monolayer, obtained after 220 s of evaporation, the QWS is 25 meV below the Fermi level.

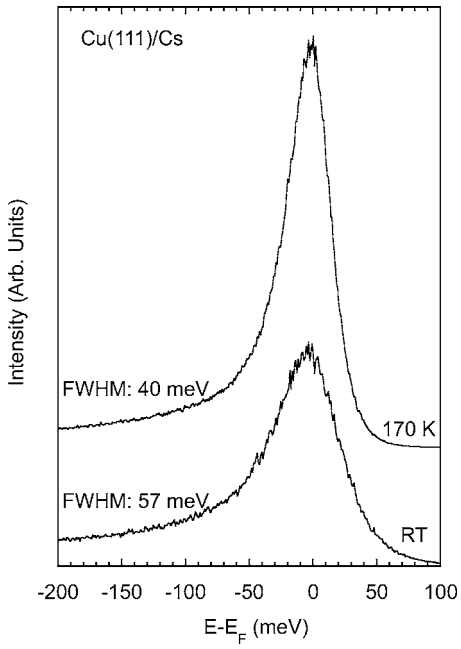

FIG. 4. Photoemission spectra recorded for the RT Cs saturation coverage. The lower spectrum is recorded with the sample at RT, and the upper spectrum after cooling the sample to 170 K. The widths given by the spectra are obtained from Lorentzians fitted to the Fermi-Dirac normalized spectra.

B. Oxygen exposure

Upon exposure to oxygen, the QWS shifts to higher energy. This effect was studied for a saturated Cs monolayer (Fig. 5). The pressure gauge was not positioned such that correct exposure values were obtained, but it could be used to increase the exposure in approximately equally large doses. As a reference regarding exposure, one may measure the work function, which passes a minimum value around 0.5 eV lower than for the Cs saturated monolayer. In previous work, the minimum was obtained after 0.4 L exposure.[25] The work-function values obtained at the different exposures are plotted in Fig. 6.

C. LEED observations

As observed for several alkali-metal adsorption systems, Cs deposition is noted as a ring pattern, which, on continued evaporation, transforms into a spot pattern.[26] The LEED pattern was registered at an electron energy (73 eV) for which the low-index Cu spots as well as Cs deposition induced changes are observed. Figure 7 shows a plot of $(d/D)^2$ versus evaporation time, where d is the diameter of the Cs induced diffraction rings observed at low coverage and, at higher coverage, the distance between opposite half-order

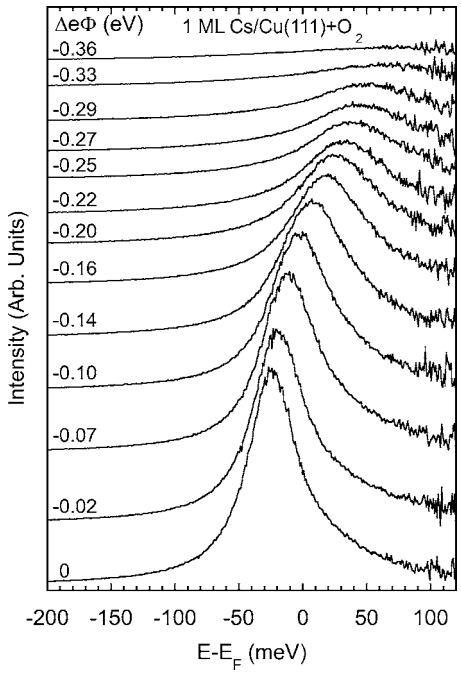

FIG. 5. Fermi-Dirac normalized photoemission spectra showing the evolution of the QWS formed in a complete monolayer Cs on Cu(111) upon O_2 exposure. The oxygen-induced work-function change is given by each spectrum. The temperature is 170 K.

spots and D is the distance between opposite substrate spots. Depending on the Cs induced pattern on the LEED display, different symbols are used in the diagram. Circles correspond to a ring pattern, circles with an inside dot to a ring pattern with azimuthal intensity variations, and filled circles to a spot pattern on the display. As can be seen in Fig. 7, $(d/D)^2$ increases linearly with deposition time until saturation of the monolayer Cs coverage at a value around 0.25, expected for a (2×2) order. The inset shows FD normalized photoemission spectra recorded in the same experimental run, which was made with the sample at 170 K. The observation of main interest is that the QWS continues to shift with increased deposition even after saturation of the diffraction angles.

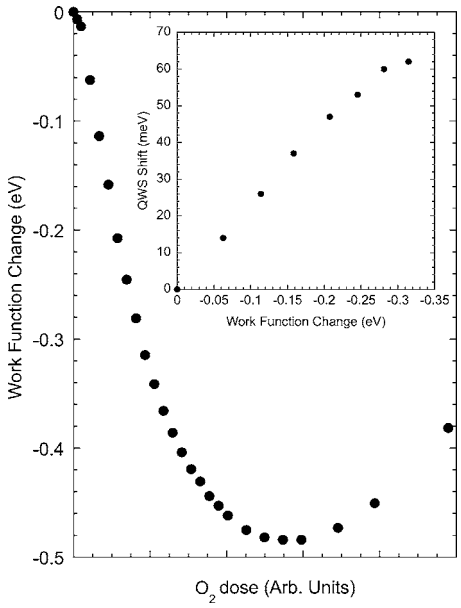

FIG. 6. The change in work function for an oxygen-exposed full monolayer Cs on Cu(111) plotted against O_2 exposure. The inset shows the shift of the QWS versus the work-function change.

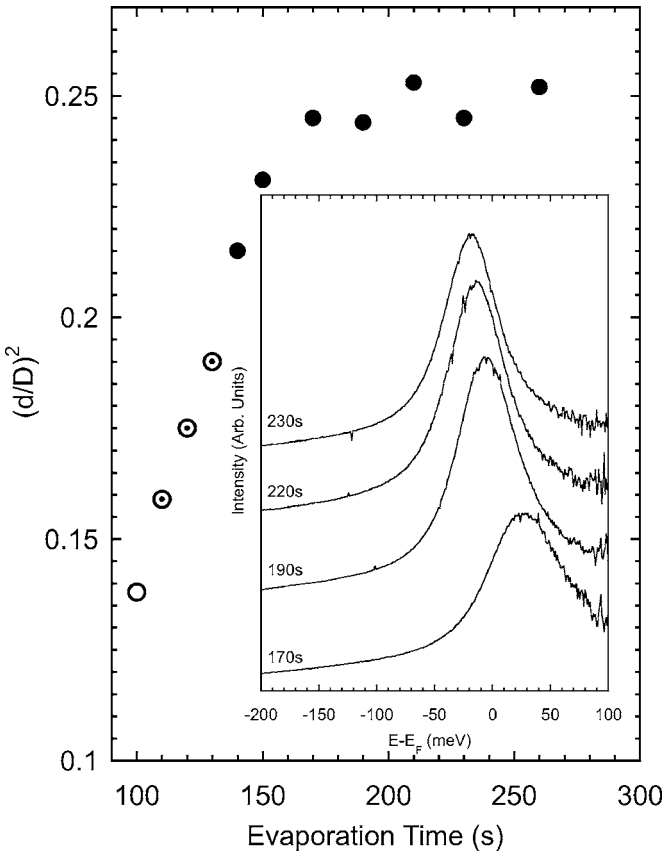

FIG. 7. The squared ratio of the distance between Cs induced features (d) and the Cu spots (D) on the LEED screen plotted against evaporation time. Different symbols are used depending on the Cs induced diffraction pattern. Circles correspond to a ring, circles with an inside dot to a ring with intensity variations, and dots to a distinct spot pattern. The inset shows Fermi-Dirac normalized photoemission spectra for coverages where the LEED pattern has saturated.

D. Surface-state shift

It was noted in a previous study that the Cu(111) surface state shifts to lower energy with increasing Cs coverage, and that the emission intensity decreases such that the state is no longer observed when it has reached the lower edge of the L gap.[14] According to the present results, however, a weak peak is resolved below the edge of the gap as the deposition is continued, indicating that the binding energy actually shifts into the resonant range (Fig. 8). The strong peak at around 2 eV binding energy is due to emission from the uppermost Cu 3d band. This emission line is, using 3.82 eV photons, revealed only at coverages near the work-function

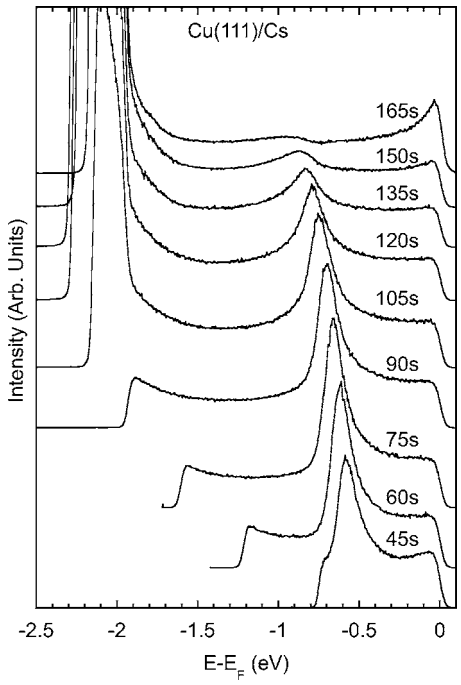

FIG. 8. Photoemission spectra showing the shift of the surface state upon Cs deposition. The evaporation time is given by the spectra. A full Cs monolayer is obtained after 225 s of evaporation. The high intensity around 2 eV binding energy in some of the spectra is due to the emission of Cu $3d$ electrons. Note how the Cs induced change of work function is reflected in spectra by a change of the low-energy cutoff. To observe the emission from states at E_F, at least a 30 s Cs deposition, corresponding to around 15% of a full monolayer, is necessary.

minimum, which is obtained after approximately half the deposition time required for obtaining a full monolayer.

E. Lattice and electron structures

Two different sites for the Cs atoms in the (2×2) monolayer on Cu(111) have been investigated, the on-top and hcp hollow sites. The lowest total energy was obtained with the Cs atoms in the on-top position with a Cs-Cu distance of 3.06 Å. This is in good agreement with previous LEED data, 3.01 ± 0.05 Å, by Lindgren *et al.*[23] The Cs atoms induce a small rumpling of the Cu surface atoms, see Fig. 9. For the relaxed structure, the Cu atom positioned under the Cs atom is pushed down by 0.13 Å.

The electronic structure and, in particular, the QWS energy relative to the Fermi level were tested by varying the smearing width σ and the number of **k** points used in the Brillouin-zone integration. The results are summarized in Table I. The conclusion from the table is that the QWS energy converges relatively slowly with respect to the number of **k** points. For the $\sigma=0.136$ eV case, we fitted the results to a damped oscillation-type function giving us an asymptotic value for the QWS energy of 0.035 eV above the Fermi level.

The band structure of the (2×2) Cs overlayer, presented in Fig. 10, along the high-symmetry directions $\bar{\Gamma}$-$\bar{M}$ and $\bar{\Gamma}$-$\bar{K}$

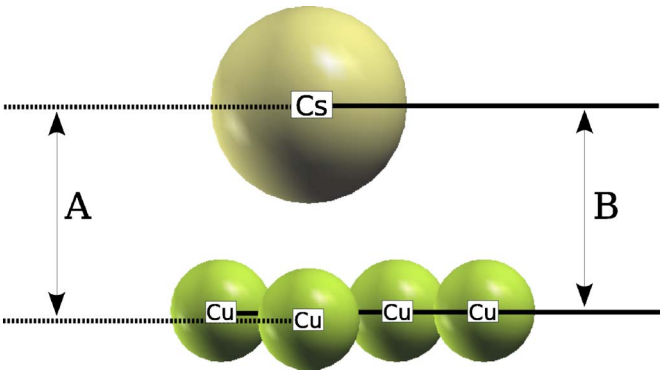

FIG. 9. (Color online) Relaxed lattice structure of (2×2)-Cs/Cu(111). The distance (A) between the Cs atom and the Cu atom positioned vertically below is 3.16 Å, and the vertical distance between Cs and the surrounding Cu atoms (B) is 3.03 Å.

of the surface Brillouin zone (SBZ) is based on calculation for $\sigma=0.136$ eV and a (10×10) Monkhorst-Pack (MP) mesh. Due to the finite thickness of the slab, each overlayer induced state is split into a doublet, represented by odd and even wave functions with respect to the center of the slab. In Fig. 10, the dark shaded area represents the clean (1×1) Cu surface projected band structure, while the light shaded area is the additional projected bulk band structure due to band folding when the (2×2) Cs layer is adsorbed. The band structure for the clean Cu(111) surface is based on calculations of an 18 atomic layer Cu slab. The mean values of the doublets of the three surface localized bands are shown by lines. The three bands are (i) the clean Cu(111) surface state, (ii) the QWS state, and (iii) the overlayer resonance state. The energy, E-E_F, of these bands in the $\bar{\Gamma}$ point is −0.39 eV [clean Cu(111) surface state], 0.033 eV (QWS), and −1.14 eV (overlayer resonance), respectively. The QWS band has a free-electron-like dispersion with an effective electron mass of $0.86m_e$. When the Cs overlayer is introduced, there is a substantial reduction of the band gap, which is illustrated by the light area in the figure.

IV. DISCUSSION

In this section, we first present details of the overlayer resonance state, referring to our photoemission spectroscopy (PES) data and calculated electron structure. Then an analysis of the monolayer lattice versus Cs exposure is presented. The coverage dependence of the QWS energy and the temperature dependence of its width with reference to the electron-phonon coupling will be discussed.

A. Overlayer resonance state

When the clean Cu(111) surface is exposed to Cs, the PES data reveal an energy downshift of the surface state (Fig. 5). After 120 s (~0.5 ML) of Cs evaporation, the state has shifted to energies below the Cu bulk band gap. The crossing of the gap edge is accompanied by a broadening of the line since the state couples to Cu bulk states. Continued Cs evaporation leads to an additional shift and broadening of the

TABLE I. Convergence test of the QWS energy, E-E_F (eV), in the $\bar{\Gamma}$ point with respect to selected **k** points used in the Brillouin-zone integration and with respect to the Methfessel-Paxton smearing width, σ (eV). The **k** points are given in terms of Monkhorst-Pack (MP) mesh with the corresponding number of **k** points in the irreducible Brillouin zone.

	MP-mesh	(6×6)	(8×8)	(10×10)	(12×12)	(14×14)
σ	No. of **k** points	13	21	31	43	57
0.680			0.082			
0.408			0.058			
0.340			0.050			
0.272		0.047	0.040	0.048	0.052	
0.136		0.062	0.013	0.033	0.054	0.031

line. The state is now better described as an overlayer resonance characteristic of the monolayer rather than as a downshifted surface state. The resonance has its origin in the free-electron-like energy-band characteristic of a freestanding, close-packed Cs monolayer, which, according to the calculations of Wimmer, extends 1.28eV below E_F.[27] The integrity of this band is thus maintained upon adsorption of the monolayer though the states are broadened due to hybridization with copper states.

The calculated overlayer resonance band along the $\bar{\Gamma}$-$\bar{M}$ direction is shown in Fig. 11 together with the squared magnitude of the wave function at specific points. In the $\bar{\Gamma}$ point, the state is spread over the Cu layers and the Cs overlayer, with not much of an overlayer resonant character. However, as one moves out toward the $\bar{M}$ point, the resonance character develops. In point A, about two-thirds of the distance to $\bar{M}$, a substantial part of the state is localized to the Cs layer. The increasing weight in the Cs overlayer as the SBZ edge is approached is seen at point B. Further characteristics of the band which support the labeling—overlayer resonance—is the absence of a node of the wave function in the Cs layer, which is also the case for the lowest band of the unsupported (2×2) Cs monolayer.[27]

The resonance character of an alkali-metal overlayer state is clearly revealed by applying an embedding method with a semi-infinite substrate. Such a calculation was recently reported for a full monolayer of Na on Cu(111).[7] This monolayer has a structure which may be approximated with a (3×3) lattice and four Na atoms in the cell. The discussion in that paper is focused on the energies and dispersion of the strongly confined states and the image potential states with energies high in the Cu L gap. Here we note that the Na projected density of states for different **k** points along symmetry lines in the Brillouin zone of the adlayer, in addition, shows resonances (Fig. 2 in Ref. 7). By reading off the energies of the resonances, one finds $E(k)$ branches with a nearly free-electron dispersion. This is shown in Fig. 12, where the energy is plotted versus the square of the wave vector for the resonances. The resonance band extends 1.5 eV below E_F and the band mass is $0.93m_e$. This may be compared with the filled bandwidth of 2.12 eV calculated for a freestanding monolayer of Na.[27]

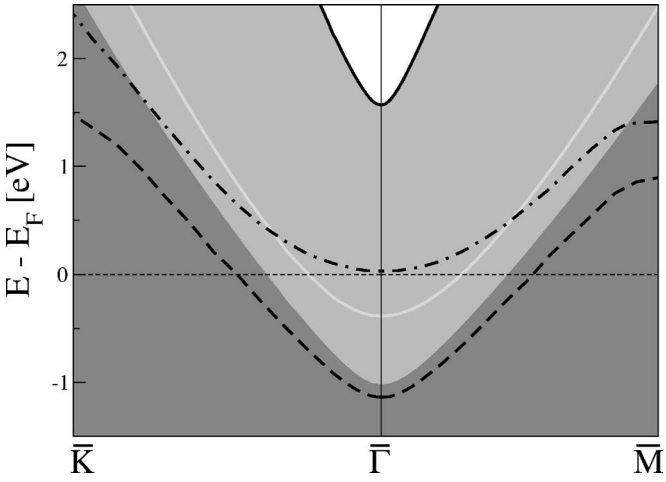

FIG. 10. Band structure of (2×2)-Cs/Cu(111) along the high-symmetry directions $\bar{\Gamma}$-$\bar{M}$ and $\bar{\Gamma}$-$\bar{K}$ in the surface Brillouin zone. The dark shaded area represents the clean Cu(111) surface projected bulk band structure and the light shaded area the additional projected bulk band structure due to band folding when the (2×2) Cs layer is adsorbed. The solid bright line represents the surface-state band, of the clean Cu(111) surface, the dashed-dotted line the QWS band, and the dashed line the overlayer resonance band.

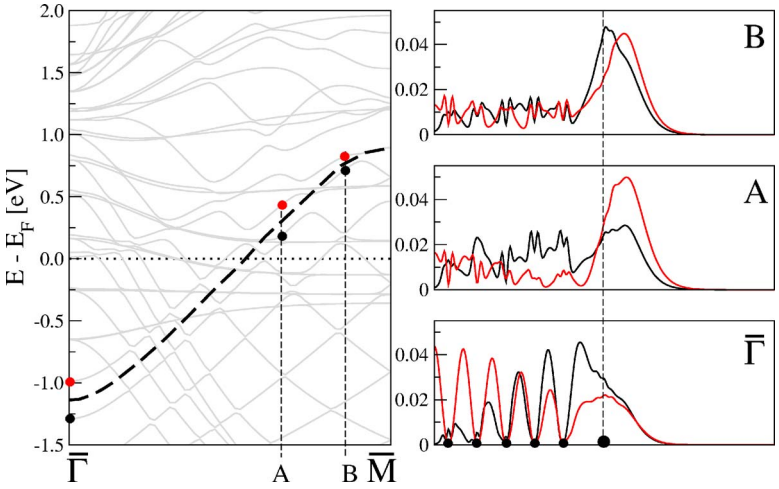

FIG. 11. (Color online) Electron structure of the overlayer resonance state. To the left, the band structure in the $\bar{\Gamma}$-$\bar{M}$ direction, and to the right, the even (red) and odd (black) squared magnitude of the wave function, averaged in planes parallel to the surface, at different locations along the overlayer resonance band.

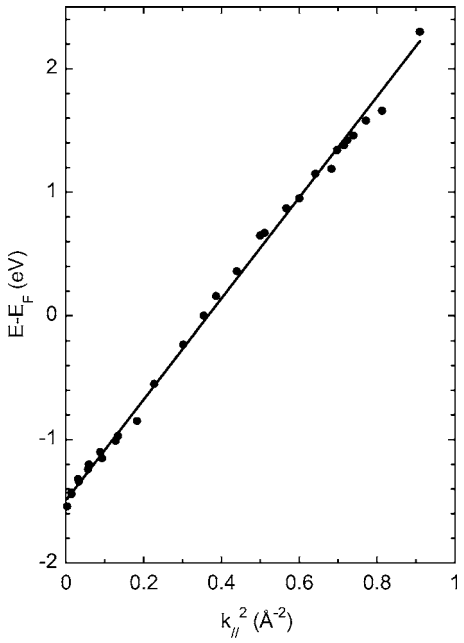

FIG. 12. Energy versus squared parallel wave vector for the resonance state formed in 1 ML Na on Cu(111). The data points are obtained by reading off the peak positions in the density of state curves presented by Butti *et al.* (Ref. 7). The straight line is a fit to the data points.

To conclude, our picture, based on PES data and electron structure calculations, is that the surface state shifts in energy upon alkali-metal adsorption and eventually turns into a resonance characteristic of the overlayer at high monolayer coverage. This view is supported by the calculation for Na on Cu(111) by Butti *et al.*,[7] according to our analysis of their data.

B. QWS-shift and LEED observations

The coverage dependence of the QWS energy is quite similar to the observations for Na and Li monolayers.[5,28] The saturation energy in the monolayer range is below the Fermi level, but closer to it for Cs (E_F-25 meV) than for Li (E_F-135 meV) (Ref. 6) or Na (E_F-97 meV).[14] The energy obtained for Na with STS is (E_F-127 meV).[29] There are two general reasons why different energies may be obtained with the two methods. Using STS, a much smaller selected area is probed and the perturbation of the sample is different. If a wide terrace is chosen, the lateral confinement will be less significant and will give a lower energy than when a large area is probed. This could explain the difference between STS and photoemission energies for the Na case. For Cs this explanation is not applicable since the STS gives a higher energy (E_F+40 meV).[9] This energy was measured at 5 K for a sample cooled after deposition at RT of an amount that gave a (2×2) LEED pattern at RT. This energy may be compared with the saturation ~10 meV above E_F in the present experiment for a sample prepared at RT and measured at RT or 170 K. Assuming an insignificant energy shift between 170 and 5 K and constant sticking probability, the deposition time dependence observed here for the QWS energy would suggest that the tunneling results are representative of around 93% of the saturation coverage at RT. According to the present observations, a (2×2) order is observed for a range of coverages and, for the QWS energies observed with STS, the coverage is within this range. Our LEED observations made with the sample at 170 K suggest an inhomogeneous Cs surface density at high monolayer coverages. The lattice parameter saturates at a value which deviates insignificantly from that of the (2×2) order, but the QWS energy continues to change with evaporation even after saturation of the lattice parameter. A possible explanation for this may be that completion of the layer occurs via occupation of vacant sites in the layer. A STM image for the (2×2) layer indicates that there are rather large holes in the Cs film (Fig. 5 in Ref. 24), but this observation was made at 5 K. One may note that the fraction of the surface area covered by Cs islands is not far from the above coverage estimate based on the QWS energies.

The details discussed above are of interest for the resonance broadening of the QWS, indicated by the theoretical evaluation of the STS data, which was based on the assumption of $p(2\times2)$ order for the Cs atoms. The present results indicate that this assumption is valid. The structure is very close to this order even though the RT saturation coverage is lower than a full monolayer. For the (2×2) overlayer considered by the authors, the QWS couples to Cu bulk states along the *L-X* direction, but this mechanism should apply also for other overlayer coverages and orders. If, for example, the overlayer is sparser and rotated compared to the (2×2) overlayer, the only difference would be that the overlayer states couple to states some distance away from the *L-X* line. The point of this comment is that the resonance mechanism is expected to be rather robust with respect to deviations from the ideal order for the overlayer. We note that the mechanism should be applicable also at low Cs coverage and then to the Cu(111) surface state. This is clearly the case when the adsorbate forms ordered structure found with STM at low Cs coverage and temperature.[9] At higher temperature, the diffraction rings observed with LEED define the scattering vectors which couple the surface state at $\bar{\Gamma}$ to bulk states on a cylinder on the *L-X* direction.

An outstanding question concerns to what extent the inhomogeneity of the Cs monolayer affects not only the QWS energy but also adds one more contribution to the measured linewidth.

C. Width of QWS

Although an inhomogeneous density and elastic scattering[9] may contribute, we expect that the phonon processes give important contributions to the linewidth of the QWS peak. A sign of this is the narrowing of the peak between 295 and 170 K, from 57 to 40 meV (FWHM). At the saturated Cs coverage, the QWS binding energy is stable close to the Fermi level for these temperatures (see Fig. 4). The phonon-induced linewidth is then given by[30]

$$\Gamma_{ep}(T) = 2\pi\hbar \int_0^{\omega_m} \alpha^2 F(\omega)[1 + 2n(\omega;T) + f(-\epsilon_b + \omega;T) - f(-\epsilon_b - \omega;T)]d\omega \simeq 4\pi\hbar \int_0^{\omega_m} \frac{\alpha^2 F(\omega)}{\sinh\left(\frac{\hbar\omega}{k_B T}\right)} d\omega, \quad (1)$$

where $\alpha^2 F(\omega)$ is the electron-phonon coupling Eliashberg function associated with the QWS, f and n the electron and phonon distribution functions, respectively, ω_m the maximum phonon frequency of the system, and ϵ_b the QWS binding energy. As long as the $\hbar\omega_m \leqslant k_B T$, the width is approximately linear in temperature

$$\Gamma_{ep}(T) = 4\pi\hbar \int_0^{\omega_m} \frac{\alpha^2 F(\omega)}{\hbar\omega} d\omega k_B T = 2\pi\lambda_0 k_B T, \quad (2)$$

where λ_0 is the zero-temperature electron-phonon coupling parameter. At this point, we actually do not know $\alpha^2 F(\omega)$ for the QWS and, thus, we have no information about the maximum frequency of the phonons which are assisting in the filling of the QWS photohole in the $\bar{\Gamma}$ point. If we take the bulk copper Debye energy ($\hbar\omega_D = 30$ meV) as an upper limit for the maximum phonon energy, Eq. (1) gives a slight reduction of the slope of the width versus temperature at the lower temperature $T = 170$ K ($k_B T = 15$ meV) in comparison with the slope at 295 K. Equation (2) is then adjusted by a factor ξ

$$\Gamma_{ep}(T) = 2\pi\xi\lambda_0 k_B T, \quad (3)$$

where $\xi = (1/2)(\hbar\omega/k_B T)^2[\cosh(\hbar\omega/k_B T) - 1]^{-1}$, with the property $\xi \to 1$ as $T \to \infty$. From the fitting to our two measured widths, assuming constant additional non-phonon-induced broadening, we obtain the low-temperature lambda value $\lambda_0 = 0.18$. Equation (3) then yields $\Gamma_{ep}(170\ \text{K}) = 12$ meV and $\Gamma(295\ \text{K}) = 29$ meV. Comparing these values with the measured widths gives an estimate of the additional contributions from elastic broadening, inelastic electron-electron scattering, and inhomogeneous broadening of 28 meV.

Applying the Debye model, $\alpha^2 F(\omega) = \lambda_0 \left(\frac{\omega}{\omega_D}\right)^2$, and experimental QWS binding energy $\epsilon_b = 25$ meV, the zero-temperature ($T = 0$) phonon-induced width is determined by Eq. (1). The upper integration limit is now given by $\epsilon_b/\hbar$ as no phonons with higher frequencies can be emitted at $T = 0$. We then obtain

$$\Gamma_{ep}(0) = 2\pi\hbar \int_0^{\epsilon_b/\hbar} \alpha^2 F(\omega) d\omega = \frac{2}{3}\pi\lambda_0 \frac{\epsilon_b^3}{\hbar^2 \omega_D^2} \simeq 7\ \text{meV}. \quad (4)$$

This value is approximately the same as estimated in the previous study of this system,[9] 7.5 ± 3 meV. The fact that the data of a local probe measurement, STS, are consistent with our PES data regarding the phonon-induced linewidth suggests that the present data are not much affected by an inhomogeneous adatom density across the much larger area probed. Still, we want to emphasize that the phonon-induced width estimated here and in the work by Corriol *et al.*[9] is not conclusive, as they both are partly based on an oversimplified Debye model for the Eliashberg function. Preliminary phonon calculations of the system indicate low-frequency surface localized modes which might be of crucial importance for an appropriate Eliashberg function of the QWS.[31]

D. Oxygen exposure

First to note is that the integrity of the QWS is maintained upon oxygen exposure. The gradual energy shift is in accordance with a model presented in a previous work[25] based on a gradual downshift observed for the plasmon loss energy, namely, that oxygen acts as a diluter of the electron gas in the Cs layer. The Cs atoms collectively transfer electrons to the oxygen atoms such that a rather homogeneous electron gas with reduced density is obtained. The upward shift of the QWS means that part of the transferred charge is donated via the depopulation of the QWS band. In concert with the energy shift, the line broadens from 44 meV FWHM at zero exposure to 105 meV when the QWS energy is 45 meV above E_F. This is in contrast to a pure Cs overlayer where the line is only marginally broader when found at 45 meV above E_F than when it is observed for full monolayer coverage at 25 meV below E_F. While the QWS is clearly seen in spectra at 100 meV above E_F for the pure Cs overlayer, the broader line for the oxygen exposed Cs together with a lower intensity makes it difficult to observe for state energies higher than 75 meV above E_F at 170 K.

The upshift of the monolayer QWS upon oxygen exposure provides part of the explanation for the decrease of the work function. The work function reflects the electron density of a free-electron metal.[32] For a film, the work function is also sensitive to the balance between populated states with long and short tails into vacuum.[33] Oxygen exposure changes both, such that the work function is reduced. The plasmon energy of the overlayer is reduced gradually with increasing exposure.[25] This signals that the electron gas in the film becomes thinner, which results in a lower work function. The reduction is particularly large if the electrons removed from the film extend far into vacuum.[33] This applies to the QWS, which has a node in the film. This is seen in Fig. 13, where the square of the magnitude of the wave function of the QWS is shown in the $\bar{\Gamma}$ point. As the QWS band is depopulated on oxygen exposure, this will thus give a stronger contribution to the work-function change than the removal of electrons from the resonant states below the L gap.

V. CONCLUSIONS

The electronic structure of Cs/Cu(111) at 170 K and full monolayer coverage is characterized by a QWS band extending 25 meV below E_F and a resonance band extending to energies below the edge of the Cu L gap. At RT the QWS energy is around 35 meV higher than at 170 K, which is ascribed to a smaller saturation coverage at RT. A LEED pattern characteristic of (2×2) order is observed in a range of monolayer coverages, giving the QWS energies in the range from $E_F - 25$ meV to $E_F + 50$ meV. This is in accor-

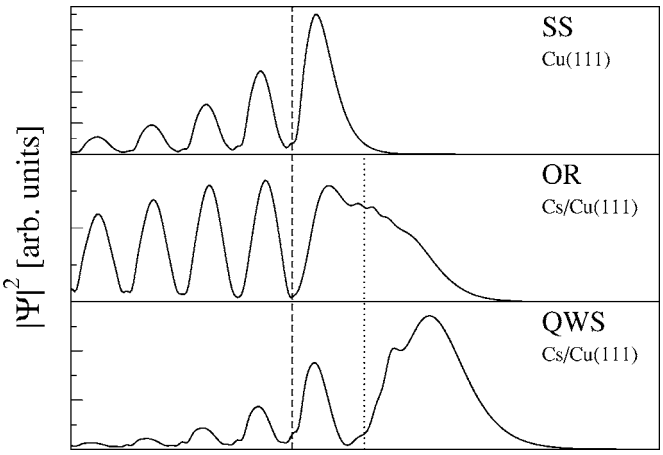

FIG. 13. The average of the squared magnitude of the even and odd wave functions of surface localized states in the $\bar{\Gamma}$ point. From the top: surface state (SS) of clean Cu(111) and overlayer resonance (OR) state and quantum well state (QWS) of (2×2)-Cs/Cu(111). The horizontal axis (left to right) ranges from the slab center toward the vacuum region. The dashed line represents the mean position of the first Cu layer and the dotted line the position of the Cs atom.

dance with the QWS energy E_F+40 meV obtained with STS by Corriol *et al.*[9] and the energy obtained from the present and previously reported[9] first-principles calculations. Our data give no clear demarcation of the optimum coverage for the Cs $p(2\times2)$ structure. A likely interpretation, which would reconcile the continued shift of the QWS energy with the constant LEED angles, is that this structure is only complete near full monolayer coverage and that the incomplete monolayer has vacancies.

The gradual downshift of the Cu(111) surface state to energies below the Cu L gap suggests that the surface state gradually transforms with increasing coverage to an overlayer resonance. Such a resonance is predicted by the present calculations for Cs/Cu(111) and recently also for Na/Cu(111).[7]

Regarding the resonance broadening proposed for QWS,[9] characteristic of ordered Na and Cs monolayers on Cu(111), we point out that the mechanism should be relevant also for less ordered overlayers as exemplified by alkali-metal overlayers at low and intermediate coverages. This means that a coverage-dependent resonance broadening is expected for the Cu(111) surface state as this is downshifted upon alkali-metal adsorption. For the monolayer QWS, the width is predicted to depend mildly on deviations from the ideal ordered structure considered in the previous work.[9] An indication of the rather modest broadening induced by disorder is that the integrity of the monolayer QWS is maintained upon oxygen exposures sufficient to give appreciable energy shifts.

[1] S.-Å. Lindgren and L. Walldén, in *Electronic structure*, edited by S. Holloway, N. V. Richardson, K. Horn, and M. Scheffler, Handbook of Surface Science Vol. 2 (Elsevier Science, Amsterdam, 2000).
[2] S. R. Barman, P. Häberle, K. Horn, J. A. Maytorena, and A. Liebsch, Phys. Rev. Lett. **86**, 5108 (2001).
[3] D. Heskett, K.-H. Frank, E. E. Koch, and H. J. Freund, Phys. Rev. B **36**, 1276 (1987).
[4] I. Lindau and L. Walldén, Phys. Scr. **3**, 77 (1971).
[5] A. Carlsson, S.-Å Lindgren C. Svensson, and L. Walldén, Phys. Rev. B **50**, 8926 (1994).
[6] D. Claesson, S.-Å Lindgren, and L. Walldén, Phys. Rev. B **60**, 5217 (1999).
[7] G. Butti, S. Caravati, G. P. Brivio, M. I. Trioni, and H. Ishida, Phys. Rev. B **72**, 125402 (2005).
[8] J. M. Carlsson and B. Hellsing, Phys. Rev. B **61**, 13973 (2000).
[9] C. Corriol, V. M. Silkin, D. Sánchez-Portal, A. Arnau, E. V. Chulkov, P. M. Echenique, T. von Hofe, J. Kliewer, J. Kröger, and R. Berndt, Phys. Rev. Lett. **95**, 176802 (2005).
[10] for a review, see M. Grioni, Ch. R. Ast, D. Pacilé, M. Papagna, H. Berger, and L. Perfetti, New J. Phys. **7**, 106 (2005).
[11] S.-Å Lindgren and L. Walldén, Surf. Sci. **89**, 319 (1979).
[12] S.-Å Lindgren and L. Walldén, Phys. Rev. B **38**, 3060 (1988).
[13] S.-Å Lindgren and L. Walldén, Solid State Commun. **28**, 283 (1978).
[14] A. Carlsson, B. Hellsing, S.-Å Lindgren, and L. Walldén, Phys. Rev. B **56**, 1593 (1997).
[15] S. Ogawa, H. Nagano, and H. Petek, Phys. Rev. Lett. **82**, 1931 (1999).
[16] P. Johansson, G. Hoffmann, and R. Berndt, Phys. Rev. B **66**, 245415 (2002).
[17] G. Hoffmann, R. Berndt, and P. Johansson, Phys. Rev. Lett. **90**, 046803 (2003).
[18] S. Baroni, A. Dal Corso, S. de Gironcoli, P. Giannozzi, C. Cavazzoni, G. Ballabio, S. Scandolo, G. Chiarotti, P. Focher, A. Pasquarello, K. Laasonen, A. Trave, R. Car, N. Marzari, and A. Kokalj, http://www.pwscf.org/
[19] D. Vanderbilt, Phys. Rev. B **41**, 7892 (1990).
[20] J. P. Perdew, K. Burke, and M. Ernzerhof, Phys. Rev. Lett. **77**, 3865 (1996).
[21] P. Giannozzi, F. De Angelis, and R. Car, J. Chem. Phys. **120**, 5903 (2004).
[22] M. Methfessel and A. T. Paxton, Phys. Rev. B **40**, 3616 (1989).
[23] S.-Å Lindgren, L. Walldén, J. Rundgren, P. Westrin, and J. Neve, Phys. Rev. B **28**, 6707 (1983).
[24] Th. von Hofe, J. Kröger, and R. Berndt, Phys. Rev. B **73**, 245434 (2006).
[25] S.-Å Lindgren and L. Walldén, Phys. Rev. B **22**, 5967 (1980).
[26] R. D. Diehl and R. McGrath, Surf. Sci. Rep. **23**, 46 (1996).
[27] E. Wimmer, J. Phys. F: Met. Phys. **13**, 2313 (1983).
[28] A. Carlsson, D. Claesson, G. Katrich, S.-Å Lindgren, and L. Walldén, Phys. Rev. B **57**, 13192 (1998).
[29] J. Kliewer and R. Berndt, Phys. Rev. B **65**, 035412 (2001).
[30] B. Hellsing, A. Eiguren, and E. V. Chulkov, J. Phys.: Condens. Matter **14**, 5959 (2002).
[31] A. Nojima and B. Hellsing (unpunblished).
[32] N. D. Lang and W. Kohn, Phys. Rev. B **3**, 1215 (1971).
[33] J. K. Schulte, Surf. Sci. **55**, 427 (1976).